ingegneria sismica
International Journal of Earthquake Engineering
Anno XLIII - Num. 3 - 2026

# Consolidation of Soft Ground Improved by Biodegradable Prefabricated Vertical Drains with Time-Dependent Discharge-Capacity Decay: A Field-Validated Finite-Element Study

*Lewen Cheng*[1,*]

[1] Key Laboratory of Ministry of Education for Geomechanics and Embankment Engineering, Hohai University, Nanjing 210098, China

**SUMMARY:** *Biodegradable prefabricated vertical drains (PVDs) are an emerging green alternative to conventional plastic drains, but their core material degrades during service, so the drain discharge capacity decays with time and the well-resistance effect intensifies; consolidation analyses that assume a constant discharge capacity therefore cannot reproduce the true field behaviour. Unlike previous analyses that assume an exponential or polynomial decay, this paper calibrates the discharge-capacity decay directly from laboratory tests and embeds it in a field-validated finite-element (FE) consolidation model. Laboratory accelerated-degradation and longitudinal discharge-capacity tests provided the measured decay data; after comparison with an exponential model, a logistic function with upper and lower asymptotes was selected to describe the decay, and was converted, via Darcy's law and the equivalent-hydraulic-radius method, into a time-dependent decay function of the drain permeability. Because general-purpose FE codes cannot vary a parameter continuously in time, a staged-assignment method was proposed that discretises the continuous decay curve into successive stages and updates the drain permeability stage by stage. Using the Soft-Soil constitutive model for the non-linear compressibility of dredged silty clay, the model was validated against field settlement and excess-pore-pressure measurements at Meishan Port, Ningbo, and then applied to sensitivity analyses of the drain spacing, decay rate and decay amplitude and a 1000-day long-term prediction, providing a calibratable and field-verifiable reference for the design-parameter selection of biodegradable-PVD ground improvement.*

***KEYWORDS:*** *biodegradable prefabricated vertical drain; discharge-capacity decay; well resistance; finite element method; consolidation; parametric analysis*

# 1 Introduction

With the rapid development of offshore artificial islands, port construction and land reclamation, the demand for treating deep dredged silty-clay foundations has grown steadily. Conventional plastic prefabricated vertical drains (PVDs) effectively accelerate the consolidation of soft soils, but because they are made of non-degradable polymers such as polyethylene and polypropylene, they remain in the ground for a long time after construction, causing "white pollution" and interfering with subsequent excavation and pile installation. Biodegradable PVDs, manufactured by combining polylactic acid (PLA), poly(butylene adipate-co-terephthalate) (PBAT) and plant fibres, can gradually degrade into harmless products once their drainage function has been fulfilled. Such drains meet the demand for

*231304010005@hhu.edu.cn
https://doi.org/10.65102/is20261303 Published:20 November, 2026

sustainable drainage materials under the goals of green geotechnics and carbon neutrality and therefore have promising engineering prospects [1].

The key engineering concern for biodegradable PVDs, however, is that as the core material degrades, its longitudinal discharge capacity decreases with time and the well-resistance effect intensifies accordingly. If degradation is too rapid or the residual discharge capacity is insufficient, the drainage function may weaken before primary consolidation is complete, thereby impairing the improvement effect. Reasonably characterising the time-dependent decay of the discharge capacity and incorporating it into consolidation analysis is thus a critical step toward the engineering application of this material. In terms of consolidation theory, radial consolidation analysis of vertical-drain foundations has developed through studies of clay-soil consolidation and practical solutions incorporating smear and well resistance; Onoue further provided a rigorous displacement-based solution accounting for both well resistance and smear [2-4]. For time-dependent drainage, Kim et al. used laboratory tests and field settlement data to develop and verify a time-dependent well-resistance factor [5]; Indraratna et al. treated the discharge capacity of natural-fibre drains as an exponential or polynomial function of time and obtained the corresponding analytical solutions [6]; and Walker et al. considered non-Darcian flow together with void-ratio-dependent compressibility and permeability [7]. These analytical approaches rely on different idealisations of strain, soil behaviour, loading and drainage; their direct application to non-linear dredged silty clay, staged construction loading and design-oriented parametric sweeps therefore requires care.

The finite element (FE) method can largely overcome these limitations. The simplified modelling approach of Chai et al., which represents drain-improved soil as an equivalent homogeneous layer, has been widely adopted in mainstream FE software; Walker and Indraratna applied the spectral Galerkin method to multilayer consolidation with vertical drains, including depth-dependent well resistance [8-9]; and Nguyen et al. developed a numerical framework for the service-performance degradation of biodegradable drains, revealing that material durability must be matched to the engineering functional period [10]. In parallel, finite-element analyses incorporating smear and well resistance have been compared with field measurements for embankments on soft clay [11], while advanced constitutive models have been assessed in vertical-drain simulations and applied to a full-scale embankment case history [12]. Nevertheless, general-purpose geotechnical FE codes such as PLAXIS do not provide a built-in facility for varying a material parameter continuously with time; the drain permeability is treated as constant within a single calculation phase. How to reasonably introduce the continuous degradation of drain performance into a numerical model therefore remains the key technical difficulty in simulating this class of problems. Compared with existing numerical consolidation studies and dedicated drain-degradation simulations, the novelty of the present work lies less in the numerical technique than in the physical problem it captures and the way it is calibrated and verified: the time-dependent discharge-capacity decay of a biodegradable drain is characterised directly from laboratory accelerated-degradation and discharge-capacity tests by a logistic function with upper and lower asymptotes—rather than an assumed exponential or polynomial form—and is embedded in a consolidation model with a soft-soil non-linear constitutive law that is validated against field settlement and excess-pore-pressure measurements. That the same decay law can additionally be introduced into general-purpose commercial FE software through a staged-assignment scheme, without secondary development, makes the framework readily transferable to routine engineering practice.

Accordingly, taking the dredged silty-clay foundation at Meishan Port, Ningbo, as the engineering background, this paper establishes an FE consolidation model that accounts for the time-dependent decay of the drain equivalent permeability. First, based on laboratory

accelerated-degradation and discharge-capacity test data, a logistic function is selected to formulate the time-dependent decay equation of the discharge capacity, which is then converted into a time-dependent decay function of the drain equivalent permeability. A staged-assignment method is proposed to realise the numerical representation of the continuous permeability decay. The soft-soil constitutive model is used to describe the non-linear compressibility of the soil, and the results are validated against field measurements. Finally, sensitivity analyses of the drain spacing d, the decay-rate parameter $\lambda$ and the decay-amplitude parameter $\beta$ are carried out, together with a long-term settlement prediction, to provide quantitative guidance for engineering design.

The main contributions of this study are threefold: (1) a logistic discharge-capacity decay law for biodegradable PVDs, calibrated from laboratory accelerated-degradation and JTG E50 discharge-capacity tests and converted into a drain-permeability decay function; (2) a staged-assignment scheme that embeds this time-dependent well resistance into a general-purpose FE consolidation model with a soft-soil non-linear constitutive law; and (3) field validation at Meishan Port together with a parametric study of the drain spacing and the decay-rate and decay-amplitude parameters and a 1000-day prediction, providing quantitative guidance for the design of biodegradable-PVD ground improvement.

# 2 Discharge-Capacity Decay and Permeability Conversion Model

## 2.1 Degradation Test and Data Acquisition

The biodegradable PVD used in this study is a commercially available integral drain manufactured from PLA, PBAT and plant fibres, with a total degradable-component content of about 15%–25%. To obtain discharge-capacity decay data representative of field conditions, an "accelerated degradation–in-situ-soil calibration–discharge-capacity measurement" scheme was adopted. First, considering that the pore water of dredged soft soil is generally weakly alkaline and that an alkaline environment simultaneously promotes hydrolysis of the PLA ester bonds and decomposition of the plant fibres, accelerated degradation was performed in a 10% (by mass) NaOH solution at a constant temperature of 20 °C; a series of specimens with weight-loss ratios distributed uniformly from 0 to about 16% was obtained by varying the immersion time. Second, the same drain was buried in undisturbed dredged silty clay collected on site for a natural-degradation control test, and, on the principle of equal weight-loss ratio, the correspondence between accelerated-degradation time and natural service time was established, so that the accelerated data could be extrapolated to the engineering time scale. The natural service time corresponding to each specimen, calibrated from the equal-weight-loss data points of the control test, is listed in Table 1.

On this basis, longitudinal discharge-capacity tests were carried out on specimens with different weight-loss ratios. The tests followed the Test Methods of Geosynthetics for Highway Engineering (JTG E50): the cumulative discharge over 24 h was measured under a normal pressure of 150 kPa and a constant hydraulic gradient of $i = 0.5$, and converted to the longitudinal discharge capacity at the standard temperature (20 °C), in $cm^3/s$. Each value is the arithmetic mean of three parallel specimens, whose measured discharge capacities showed low scatter and good repeatability. The natural service time, weight-loss ratio and measured discharge capacity of each specimen are summarised in Table 1. The discharge capacity decreases as degradation proceeds and exhibits a non-linear pattern of "slow early decline, rapid mid-stage decay and a stable residual value at the late stage".

*Table 1: Weight-loss ratio and measured discharge capacity at different natural degradation times.*

| Natural service time t (d) | Weight-loss ratio D (%) | Measured discharge capacity $q_w$ (cm³/s) |
|---|---|---|
| 0 | 0.00 | 40.00 |
| 53.3 | 2.25 | 37.33 |
| 60.0 | 2.50 | 35.40 |
| 375.0 | 10.35 | 23.10 |
| 400.0 | 10.60 | 22.30 |
| 833.3 | 15.90 | 19.70 |
| 1066.7 | 16.40 | 19.20 |

## 2.2 Formulation and Selection of the Discharge-Capacity Decay Equation

Among existing studies on PVD discharge-capacity decay, the exponential model is the most common mathematical form. It assumes that the decay rate is proportional to the current discharge capacity, i.e. dqw/dt = −α$q_w$, whose solution is

$$q_w(t) = q_{w0}e^{-\alpha t} \tag{1}$$

where $q_{w0}$ is the initial discharge capacity and α is the decay coefficient. A non-linear least-squares fit to the data in Table 1 gives α = $8.525\times10^{-4}$ $d^{-1}$ . Back-substitution shows that the model has small errors in the early degradation stage, significantly overestimates the discharge capacity in the middle stage (about 375–400 d) with relative errors of 25%–28%, and then underestimates it in the late stage (the last test point is about 16% low); moreover, as t increases the discharge capacity tends monotonically to zero and cannot reflect the physical fact that it approaches a stable residual value. This is because the exponential model assumes a constant decay rate and cannot capture the three-stage "slow–fast–stable" non-linear feature of the degradation process.

To overcome this deficiency, a logistic function with both upper and lower asymptotes was chosen to describe the discharge-capacity decay. The logistic function is a classical S-shaped curve originally used to describe growth/decay processes with a saturation limit; its "upper-asymptote–rapid-transition–lower-asymptote" shape is highly consistent, in physical mechanism, with the "initial capacity largely retained–rapid mid-stage decay–stable residual value" degradation law of biodegradable PVDs. Its reversed (decaying) form is therefore introduced to characterise the evolution of the discharge capacity $q_w$ with service time t:

$$q_w(t) = q_{max} - \frac{q_{max}-q_{min}}{1+e^{-\lambda(t-t_0)}} \tag{2}$$

where $q_{max}$ and $q_{min}$ are the upper and lower asymptotic values (the initial and residual discharge capacities), λ is the decay-rate parameter, and $t_0$ is the inflection time. Taking $q_{max}$ = 40 cm³/s and fitting the data in Table 1 gives $q_{max} - q_{min}$ = 20.8 cm³/s, λ = 0.011 $d^{-1}$ and $t_0$ = 280 d, i.e.

$$q_w(t) = 40 - \frac{20.8}{1+e^{-0.011(t-280)}} \tag{3}$$

The model has a root-mean-square error of 1.443 cm³/s and a coefficient of determination of 0.970, markedly better than the exponential model; its agreement with the measured data points is shown in Figure 1. Its physical meaning is illustrated by the asymptotic behaviour in three characteristic stages. In the early stage ($t \ll t_0$) the exponential term is large and $q_w(0) \approx$

39.09 cm³/s, close to the initial measured value, reflecting that the discharge capacity has not yet decayed appreciably. At the inflection time (t = $t_0$ = 280 d) the rate of decline is greatest, marking the transition from "slow decline" to "rapid decay". In the late stage (t ≫ $t_0$) the exponential term tends to zero and $q_w \rightarrow q_{min}$ = 19.2 cm³/s, corresponding to the baseline drainage capacity maintained by the hard-to-degrade components (part of the plant-fibre skeleton and the un-hydrolysed PLA chains), in close agreement with the value at the longest test point. It should be noted that the decay equation is fitted from seven natural-service-time points; the sample is relatively limited, so the model slightly smooths the initial rapid-decline stage and shows some deviation at individual early points, but the overall coefficient of determination of 0.970 satisfies engineering-analysis requirements. To ensure that the subsequent permeability decay function is strictly normalised at t = 0, the value of the fitted curve at t = 0, $q_w(0)$ = 39.09 cm³/s, is taken as the normalised reference discharge capacity (as distinct from the measured initial value of 40 cm³/s).

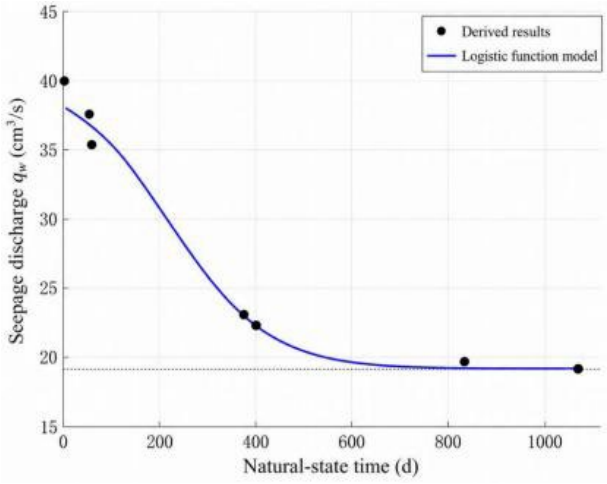


*Figure 1: Logistic-function model of discharge-capacity decay and its fit to the measured data.*

## 2.3 Discharge-Capacity–Permeability Conversion

To introduce the discharge-capacity decay law into consolidation analysis, the band-shaped drain must be idealised as a circular cross-section and the discharge capacity converted into an equivalent permeability. By the equivalent-hydraulic-radius method, the equivalent diameter is

$$d_w = \frac{2\alpha(a+b)}{\pi} \tag{4}$$

where a = 100 mm and b = 4 mm are the drain width and thickness, and the conversion coefficient α = 0.9, giving $d_w \approx 59.6$ mm. The effective flow area is

$$A_w = \frac{\eta\pi {d_w}^2}{4} \tag{5}$$

where the effective porosity η = 0.6, giving $A_w \approx 1.67\times10^{-3}$ m². By Darcy's law, at the standard hydraulic gradient i the discharge capacity and equivalent permeability satisfy $Q_w$ = kwAwi, so the discharge-capacity decay is directly converted into a permeability decay:

$$k_w(t) = k_{w0} \cdot f(t), \quad f(t) = 1 - \frac{\beta(g(t)-g_0)}{1-g_0} \tag{6}$$

where f(t) is a strictly normalised decay function: with the standard logistic function g(t) = 1/(1 + exp[−λ(t − $t_0$)]) and its initial value $g_0$ = g(0), the expression f(t) = 1 − β(g(t) − $g_0$)/(1 − $g_0$) strictly satisfies f(0) = 1 and f(∞) = 1 − β . The decay rate λ (note that it differs in meaning from the modified compression index $\lambda^*$ of the soft-soil model in Section 3.2) and the inflection time $t_0$ are inherited directly from the discharge-capacity fit (λ = 0.011 $d^{-1}$, $t_0$ = 280 d). The decay-amplitude parameter β characterises the ultimate decay magnitude and is determined by the residual ratio: f(∞) = $q_{min}/q_w(0)$ = 1 − β, giving β ≈ 0.51 for this project; the values of f(t) for each stage in Table 4 are computed from this expression. Taking the normalised reference discharge capacity $q_w(0)$ ≈ 39.09 $cm^3/s$ and i = 0.5 gives an initial equivalent permeability $k_{w0} \approx 4.68\times10^{-2}$ m/s, far larger than that of the surrounding soil, indicating that the drain has ample drainage capacity in its initial state.

# 3 Establishment of the Finite Element Model

## 3.1 Computational Domain and Geometric Model

Based on the actual conditions of the Meishan Port project, an axisymmetric FE model was built in PLAXIS 2D. The biodegradable PVDs are installed in a square pattern with a spacing of d = 1.1 m; by the equal-area principle, the drainage influence zone of a single drain is idealised as a circle of radius

$$r_e = (d^2/\pi)^{1/2} \tag{7}$$

giving $r_e$ = 0.620 m. The equivalent drain radius is $r_w$ = 0.03 m; the smear-zone radius is taken as $r_s$ = 0.06 m according to a smear ratio s = $r_s/r_w$ = 2; and the drain treatment depth is l = 18 m. The model takes the drain centre-line as the axis of symmetry, extends radially from $r_w$ to $r_e$ and vertically from the ground surface to 18 m, and is divided radially into the drain zone, the smear zone and the undisturbed zone. The vertical depth of the computational domain, 18 m, coincides with the drain treatment depth and corresponds to the main compressible layer of the test area; the underlying strata have relatively low compressibility and permeability and contribute little to the consolidation settlement, and are therefore excluded from the domain. The drain zone is assigned an equivalent permeability far higher than that of the surrounding soil and is connected to the upper permeable boundary (the sand blanket), so that pore water flowing radially into the drain is discharged to the surface through this high-permeability channel; the smear-zone permeability is reduced to reflect installation disturbance. The geometric model is shown in Figure 2, and the geometric parameters are listed in Table 2.

*Table 2: Summary of the geometric parameters of the model.*

| Parameter | Symbol | Value | Unit | Basis |
|---|---|---|---|---|
| Drain spacing | d | 1.1 | m | Design scheme |
| Influence-zone radius | $r_e$ | 0.62 | m | Equal-area calc. |
| Equivalent drain radius | $r_w$ | 0.03 | m | Hansbo equivalence |
| Smear-zone radius | $r_s$ | 0.06 | m | s = 2 |
| Radius ratio | n | 20.7 | — | $r_e/r_w$ |
| Smear ratio | s | 2 | — | $r_s/r_w$ |
| Drain length | l | 18 | m | Design scheme |
| Drain width | a | 100 | mm | Product spec. |
| Drain thickness | b | 4 | mm | Product spec. |




*Figure 2: Schematic of the geometric model.*

## 3.2 Constitutive Model and Material Parameters

To reasonably describe the marked difference in compressibility of the dredged silty clay at different stress levels and the correspondence between effective-stress growth and volumetric deformation during consolidation, the Soft-Soil model in PLAXIS was adopted. Compared with the Mohr–Coulomb model, the Soft-Soil model controls the volumetric deformation in primary loading and unloading/reloading through the modified compression index $\lambda^*$ and the modified swelling index $\kappa^*$, respectively, and is more suitable for highly compressible soft soils. The modified compression index is related to the compression index $C_c$ by

$$\lambda^* = \frac{C_c}{2.303(1+e_0)} \tag{8}$$

From oedometer tests $C_c = 0.252$ and the initial void ratio $e_0 = 1.906$, giving $\lambda^* = 0.0377$; taking the ratio of swelling to compression index $C_s/C_c = 1/5$ gives $\kappa^* = 0.0075$. Falling-head permeability tests gave a vertical permeability $k_v = 2.495\times10^{-9}$ m/s; taking $k_h/k_v = 2.0$ gives a horizontal permeability $k_h = 4.990\times10^{-9}$ m/s, and reducing this by $k_h/k_s = 3$ gives the smear-zone permeability $k_s = 1.663\times10^{-9}$ m/s. Regarding the initial stress field, the groundwater table in the test area is close to the ground surface and the dredged layer is fully saturated, so the initial vertical effective stress increases linearly with depth according to the buoyant unit weight; the preconsolidation pressure $p_c = 88$ kPa (Casagrande method) defines the initial yield surface of the Soft-Soil model, whereby the shallow foundation is slightly over-consolidated and gradually transitions to a normally consolidated state with depth. Under the 80 kPa surcharge, except for a thin near-surface layer, the vertical effective stress over most of the compressible layer exceeds $p_c$ and enters the normally consolidated (virgin-compression) range, thereby producing a large primary-consolidation settlement, consistent with the settlement magnitude obtained below. All material parameters are summarised in Table 3.

*Table 3: Summary of the material parameters.*

| Parameter | Symbol | Value | Unit | Basis |
|---|---|---|---|---|
| Modified compression index | $\lambda^*$ | 0.0377 | — | From $C_c$ |
| Modified swelling index | $\kappa^*$ | 0.0075 | — | From $C_s$ |
| Effective cohesion | c′ | 2.5 | kPa | Direct shear |
| Effective friction angle | φ′ | 7.4 | ° | Direct shear |
| Vertical permeability | $k_v$ | $2.495\times10^{-9}$ | m/s | Permeability test |
| Horizontal permeability | $k_h$ | $4.990\times10^{-9}$ | m/s | $k_h/k_v = 2.0$ |
| Initial void ratio | $e_0$ | 1.906 | — | Oedometer test |
| Preconsolidation pressure | $p_c$ | 88 | kPa | Casagrande |
| Saturated unit weight | $\gamma_{sat}$ | 15.7 | kN/m³ | Calculated |
| Poisson's ratio | ν | 0.33 | — | Empirical |
| Smear-zone permeability | $k_s$ | $1.663\times10^{-9}$ | m/s | $k_h/k_s = 3$ |
| Initial drain permeability | $k_{w0}$ | $4.68\times10^{-2}$ | m/s | From discharge cap. |

## 3.3 Staged-Assignment Method for Drain-Performance Degradation

Introducing the time-dependent permeability decay of the drain into the FE model is the core technical step of this study. Because PLAXIS 2D has no built-in facility for varying a material parameter continuously with time, and the drain permeability remains constant within a single calculation phase, a staged-assignment method was devised to approximate the continuous degradation. The basic idea is to discretise the whole consolidation process in the time domain into N successive calculation stages and, within each stage, to take the drain permeability as the decayed value at the start of that stage. Letting the start time of the j-th stage be $t_j = (j - 1)\Delta t$, the permeability of that stage is

$$k_w(j) = k_{w0} \cdot f(t_j), \quad j = 1, 2, \ldots, N \tag{9}$$

This treatment is mathematically equivalent to approximating the continuous decay curve by a step function, with an approximation error of order $O(\Delta t)$; reducing the time step keeps the error within an engineering-acceptable range. It should be noted that, because $k_w(t)$ decreases monotonically, taking the value at the start (left endpoint) of each stage is slightly higher than the true stage-averaged value, so that the well resistance is slightly underestimated and the degree of consolidation slightly overestimated; the difference in the degree of consolidation between the 20-stage and 40-stage schemes does not exceed one percentage point, indicating that this systematic bias is within an acceptable range and can be further reduced by using the stage-midpoint value if necessary. In implementation, N sets of drain material parameters differing only in permeability are created, the consolidation analysis is divided into N successive sub-phases, and before each sub-phase the drain-element properties are updated through the material-reassignment function; the initial conditions of each sub-phase automatically inherit the end state of the previous one, ensuring computational continuity. The method does not depend on the specific form of the decay function and can be extended to any f(t) and any FE platform that supports staged calculation.

According to the "slow–rapid–stable" feature of the S-shaped decay curve, non-uniform time steps were used: 30 d in the early stage (0–120 d), 20 d in the middle stage (120–320 d, covering the maximum-decay-rate region near $t_0$ = 280 d) and 30 d in the late stage (320–500 d), giving 20 calculation stages in total; the discharge capacity and converted permeability of each stage are listed in Table 4. To verify the discretisation accuracy, a refined scheme with the number of stages doubled to 40 was also built for comparison; the difference in average

degree of consolidation between the two schemes did not exceed one percentage point, confirming that the 20-stage scheme is sufficiently fine.

*Table 4: Converted drain permeability for each calculation stage.*

| Stage | Start (d) | End (d) | $q_w$(t) (cm³/s) | f(t) | $k_w$(t) (×10⁻² m/s) |
|---|---|---|---|---|---|
| 1 | 0 | 30 | 39.09 | 1.000 | 4.68 |
| 2 | 30 | 60 | 38.78 | 0.992 | 4.64 |
| 3 | 60 | 90 | 38.36 | 0.981 | 4.59 |
| 4 | 90 | 120 | 37.78 | 0.966 | 4.52 |
| 5 | 120 | 140 | 37.27 | 0.953 | 4.46 |
| 6 | 140 | 160 | 36.65 | 0.937 | 4.39 |
| 7 | 160 | 180 | 35.91 | 0.919 | 4.30 |
| 8 | 180 | 200 | 35.06 | 0.897 | 4.20 |
| 9 | 200 | 220 | 34.10 | 0.872 | 4.08 |
| 10 | 220 | 240 | 33.04 | 0.845 | 3.96 |
| 11 | 240 | 260 | 31.91 | 0.816 | 3.82 |
| 12 | 260 | 280 | 30.74 | 0.786 | 3.68 |
| 13 | 280 | 300 | 29.55 | 0.756 | 3.54 |
| 14 | 300 | 320 | 28.39 | 0.726 | 3.40 |
| 15 | 320 | 350 | 26.83 | 0.686 | 3.21 |
| 16 | 350 | 380 | 25.43 | 0.650 | 3.04 |
| 17 | 380 | 410 | 24.20 | 0.619 | 2.90 |
| 18 | 410 | 440 | 23.16 | 0.592 | 2.77 |
| 19 | 440 | 470 | 22.30 | 0.570 | 2.67 |
| 20 | 470 | 500 | 21.59 | 0.552 | 2.59 |

## 3.4 Boundary Conditions, Loading and Mesh

Mechanical boundaries: the left symmetry axis restrains radial displacement while allowing vertical movement; the right (outer) boundary of the influence zone has zero radial displacement and free vertical movement; the base restrains both vertical and radial displacement; and the top is a free surface allowing free ground settlement. Hydraulic boundaries: the top is permeable (excess pore pressure held at zero) while the base and right boundary are impermeable; as a drainage element, the finite drainage capacity of the drain is represented through the equivalent permeability $k_w$, so as to reflect the delaying effect of well resistance on consolidation.

Regarding loading, the test area was preloaded by large-area staged surcharge of quarry-run fill, with a fill height of about 5.5 m and an equivalent uniform load of about 80 kPa: roughly 0–30 d for site levelling and drainage-system installation (fill height 0), about 30–75 d for staged surcharge (fill height increasing from 0 to 5.5 m), followed by a constant-load preloading stage maintaining about 80 kPa. Considering that the staged-surcharge period (about 45 d) is short relative to the overall consolidation period of the foundation (500–1000 d), and that the focus of this paper is the effect of drain discharge-capacity degradation on medium- and long-term consolidation, the baseline case simplifies the design load of 80 kPa to a uniform surface load applied instantaneously at the start of the consolidation analysis and kept constant throughout, so as to highlight the degradation effect itself. It should be noted that this simplification, used mainly to highlight the degradation effect, alters to some extent the settlement and pore-pressure development in the early loading stage; the fact that the simulated settlement is generally lower than the field measurements is chiefly related to the

assumed soil parameters, the spatial variability of the strata and the simplification of the drainage boundaries (see Section 4), and is not governed by the loading simplification alone. The mesh was locally refined in the smear zone (no fewer than 4–5 element layers); in the undisturbed zone the radial element size did not exceed 1/10 of the influence-zone radius and the vertical element size was controlled within 1–2 m. The final scheme, determined after a mesh-convergence check, is shown in Figure 3.

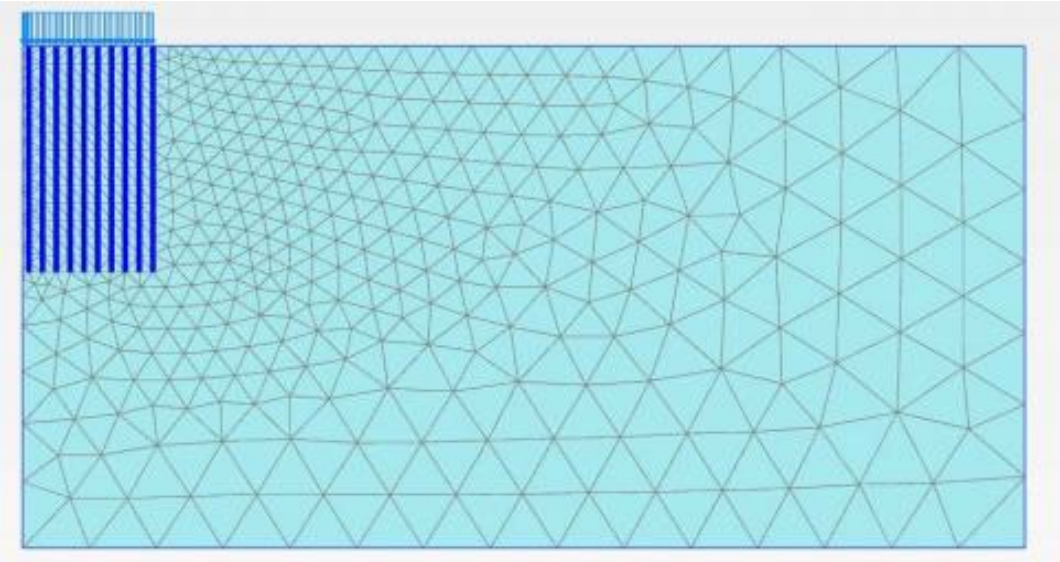

*Figure 3: Schematic of the finite element mesh.*

# 4 Numerical Results and Validation Against Field Measurements

## 4.1 Numerical Results

Following the staged-assignment method of Section 3.3, the drain permeability was reduced stage by stage while all other soil parameters, boundary conditions and loads were kept unchanged, so that the degradation effect was reflected solely through the drain equivalent discharge capacity. The development of settlement, excess pore pressure and average degree of consolidation over 500 d is given in Table 5, and the settlement and excess-pore-pressure contours at 500 d are shown in Figure 4. With $k_w$ degradation considered, the settlement increases from 0 to 743.4 mm at a gradually decreasing rate; the excess pore pressure dissipates from an initial 80 kPa to 5.51 kPa, and the average degree of consolidation reaches 93.11%. The development follows an asymptotic "fast-early, slow-late" pattern, indicating that under the present parameters the drain maintains an effective drainage function during the primary-consolidation stage.

*Table 5: Numerical results.*

| Time (d) | Settlement (mm) | Excess pore pressure (kPa) | Degree of consolidation (%) |
|---|---|---|---|
| 0 | 0.00 | 80.00 | 0.00 |
| 10 | 56.70 | 74.32 | 7.10 |
| 20 | 95.70 | 70.41 | 11.98 |
| 30 | 134.40 | 66.54 | 16.83 |
| 50 | 201.60 | 59.80 | 25.25 |
| 75 | 284.30 | 51.52 | 35.60 |
| 100 | 354.80 | 44.45 | 44.44 |
| 125 | 410.90 | 38.83 | 51.47 |
| 150 | 457.80 | 34.13 | 57.34 |
| 175 | 500.30 | 29.87 | 62.67 |
| 200 | 540.00 | 25.89 | 67.63 |
| 250 | 601.30 | 19.75 | 75.31 |
| 300 | 644.90 | 15.39 | 80.77 |
| 350 | 681.10 | 11.75 | 85.31 |
| 400 | 707.30 | 9.13 | 88.58 |
| 450 | 727.00 | 7.15 | 91.06 |
| 500 | 743.40 | 5.51 | 93.11 |

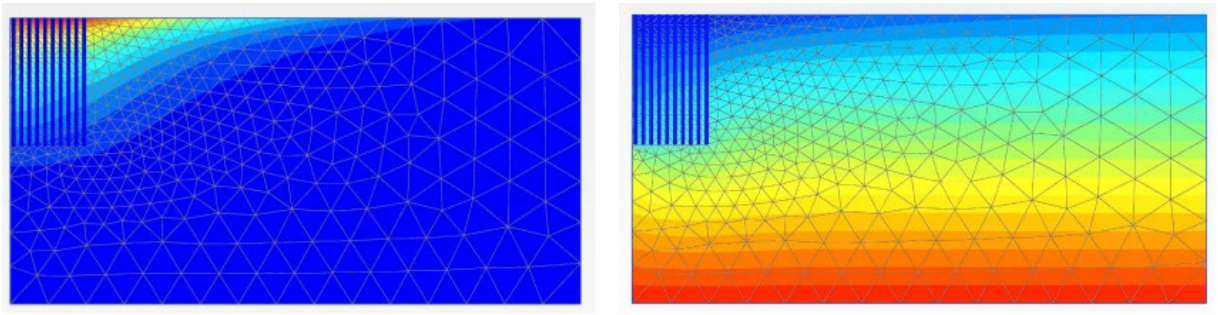

(a) Settlement (b) Excess pore pressure.

*Figure 4: Contours at 500 d*

## 4.2 Comparison of Settlement

The simulated settlement is compared with the field measurements in Table 6 and Figure 5. Both increase continuously with time and follow the same overall trend, showing that the model captures the basic settlement development of the soft-soil foundation under surcharge preloading. At every monitoring time the measured value is slightly larger than the simulated one: at 14 d the two are 109.7 mm and 80.2 mm, and at 120 d they are 536.0 mm and 403.7 mm, a relative deviation of about 24.7%. The simulated settlement is thus generally lower than the measured value. The reason is that the soil parameters of the model (compression index, permeability, coefficient of consolidation, etc.) are determined mainly from laboratory tests and, affected by sampling disturbance, size effects and spatial variability of the strata, may underestimate the actual compressibility of the field dredged silty clay; in addition, staged surcharge, construction disturbance and local drainage conditions in the field all tend to make the measured settlement exceed that of the idealised homogeneous model. It should be stressed that an underestimated settlement means that the model's prediction of the ultimate settlement is on the unsafe side; if used for post-construction settlement control, the

compressibility parameters should be calibrated against field data rather than simply regarded as "conservative".

*Table 6: Comparison of measured and simulated settlement.*

| Time (d) | Field measurement (mm) | Simulation (mm) |
|---|---|---|
| 0 | 0 | 0 |
| 14 | 109.7 | 80.2 |
| 30 | 187.2 | 134.4 |
| 75 | 384.0 | 284.3 |
| 90 | 435.0 | 322.6 |
| 120 | 536.0 | 403.7 |

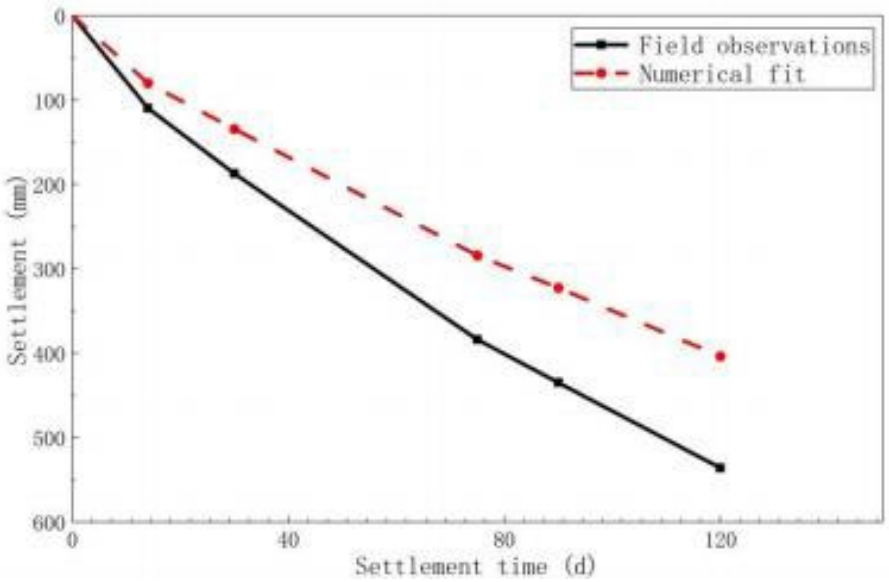


*Figure 5: Comparison of measured and simulated settlement.*

## 4.3 Comparison of Excess Pore Pressure

The excess pore pressure is compared in Table 7 and Figure 6. Both decrease overall, but the simulated curve is smoother and generally higher than the measured one, indicating that the model predicts a slower rate of pore-pressure dissipation. By 75 d the measured pore pressure has fallen to 29.9 kPa (about 62.6% dissipation), whereas the simulated value is 51.52 kPa (about 35.6% dissipation). Moreover, the measured pore pressure shows a brief rebound from 36.8 kPa to 43.6 kPa at 50–60 d, while the simulated value decreases monotonically. The differences arise mainly because staged surcharge, local pore-pressure redistribution and construction disturbance in the field cannot be fully reproduced by an idealised model, and because vertical drainage paths and local sandy interlayers provide additional drainage that accelerates the measured dissipation. Overall, the model reproduces the general trend of pore-pressure decay with time; in terms of dissipation rate the simulated value is higher and dissipation slower than measured, i.e. the prediction of the consolidation rate is conservative.

*Table 7: Comparison of measured and simulated excess pore pressure.*

| Time (d) | Field measurement (kPa) | Simulation (kPa) |
|---|---|---|
| 0 | 80.0 | 80.00 |
| 14 | 68.2 | 72.86 |
| 30 | 52.1 | 66.54 |
| 40 | 42.5 | 62.90 |
| 50 | 36.8 | 59.40 |
| 60 | 43.6 | 56.10 |
| 70 | 35.0 | 53.00 |
| 75 | 29.9 | 51.52 |

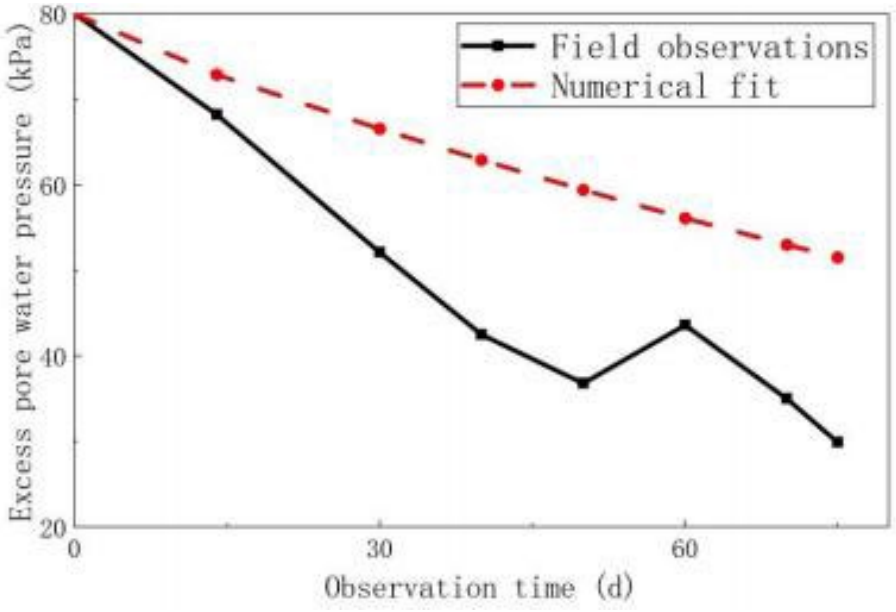


*Figure 6: Comparison of measured and simulated excess pore pressure.*

# 5 Parametric Sensitivity Analysis and Long-Term Settlement Prediction

A single-factor (control-variable) approach was used to analyse, in turn, the effects of the drain spacing d, the decay-rate parameter λ and the decay-amplitude parameter β on the development of the average degree of consolidation, and the calculation period was extended to 1000 d for long-term settlement prediction. The λ and β analyses were performed on the degradation-case FE model, whereas the drain-spacing comparison adopted the initial (undegraded) discharge capacity so as to isolate the purely geometric effect of spacing; in each analysis only the target parameter was changed while the others were kept constant, ensuring comparability. It should be noted that the magnitude of the degradation effect on the average degree of consolidation (a few percentage points; see Tables 8 and 9) is smaller than the model's prediction deviation in absolute settlement (about 25%; see Section 4). The field measurements are therefore used mainly to verify whether the model reproduces the overall trend of consolidation development, whereas the degradation effect itself is identified quantitatively through the controlled comparison with the constant-$k_w$ baseline case; the two serve different purposes. Although limited in magnitude, the degradation effect remains valuable for relative comparisons within the same model, long-service-period prediction and

biodegradable-material selection. Because the parametric analysis is set up as a self-contained comparative study, configured independently of the field-calibrated validation model of Section 4, its baseline (d = 1.1 m, λ = 0.011 $d^{-1}$, β = 0.51) 500-d degree of consolidation differs from the validated value in Table 5 (93.11%) by less than one percentage point; the conclusions drawn below therefore rest on the relative differences between cases rather than on absolute values.

## 5.1 Effect of Drain Spacing d

Starting from the baseline spacing d = 1.1 m, five cases with d = 0.8, 0.9, 1.1, 1.3 and 1.5 m were analysed, with the influence-zone radius $r_e$ recalculated by equal area and all other parameters unchanged (Figure 7). This comparison adopts the initial (undegraded) discharge capacity in order to isolate the geometric effect of spacing; accordingly, the d = 1.1 m curve here coincides with the constant-$k_w$ (non-degraded) case rather than the degraded baseline used in the λ and β analyses (Tables 8 and 9). The results show that the smaller the drain spacing, the shorter the radial drainage path, the faster the pore-pressure dissipation and the higher the average degree of consolidation at a given time: for d = 0.8 m the average degree of consolidation reaches nearly 90% at about 200 d and is essentially complete by 500 d, whereas for d = 1.5 m it is only about 75% at 500 d, with consolidation markedly delayed. Reducing the drain spacing is therefore the most direct engineering measure for accelerating the overall consolidation rate.

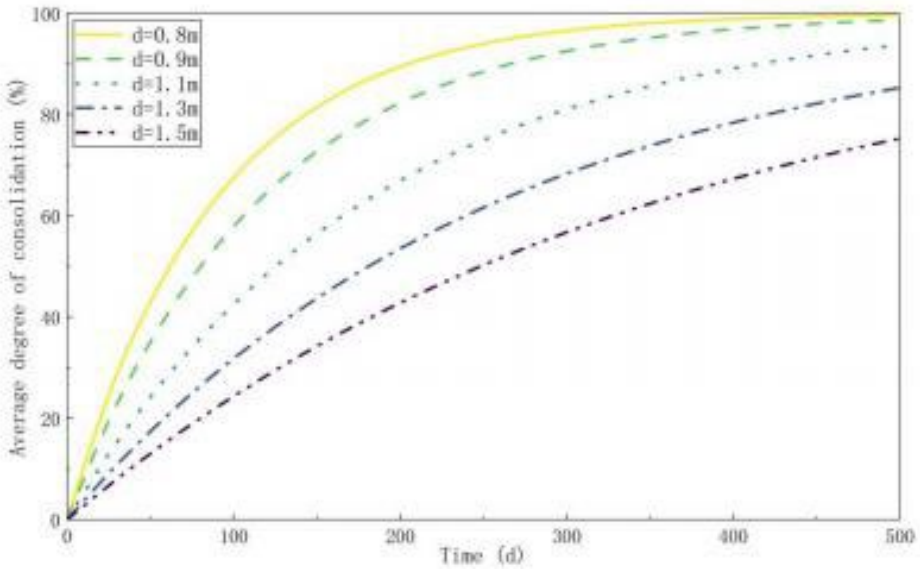


*Figure 7: Average degree of consolidation versus time for different drain spacings d.*

## 5.2 Effect of the Decay-Rate Parameter λ

The decay-rate parameter λ governs how quickly the discharge capacity falls from its initial to its asymptotic value. Starting from the baseline λ = 0.011 $d^{-1}$, five cases with λ = 0.005, 0.008, 0.011, 0.015 and 0.02 $d^{-1}$ were analysed, with the decay amplitude β and inflection time $t_0$ held constant. The differences in the degree of consolidation relative to the constant-$k_w$ case at three representative times (t = 100, 250 and 500 d) are listed in Table 8, and the corresponding trends are shown in Figure 8.

*Table 8: Difference in the degree of consolidation relative to the constant-$k_w$ case for different decay-rate parameters λ (percentage points).*

| t (d) | λ=0.005 | λ=0.008 | λ=0.011 | λ=0.015 | λ=0.02 | Constant $k_w$ |
|---|---|---|---|---|---|---|
| 100 | −1.15 | −0.76 | −0.57 | −0.27 | −0.13 | 0 |
| 250 | −1.72 | −1.45 | −1.30 | −1.05 | −0.89 | 0 |
| 500 | −1.39 | −1.49 | −1.55 | −1.65 | −1.71 | 0 |

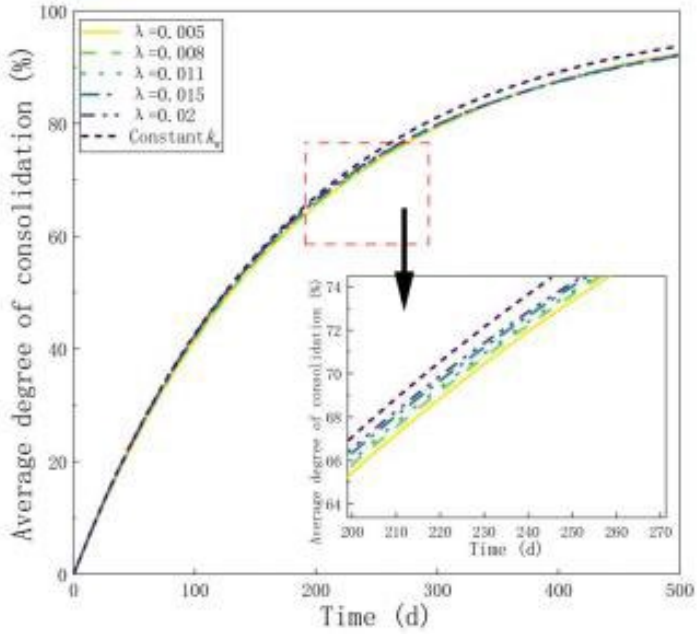


*Figure 8: Average degree of consolidation versus time for different decay-rate parameters λ.*

Table 8 shows that the influence of the decay rate λ on consolidation exhibits a time-dependent crossover. In the early-to-middle stage (t ≤ about 250 d), a smaller λ spreads the discharge-capacity decay over a longer period and initiates degradation earlier, so well resistance appears sooner and the corresponding reduction in the degree of consolidation is actually larger (at 100 d the reduction for λ = 0.005 $d^{-1}$ is about 1.15 percentage points, far exceeding the 0.13 point for λ = 0.02 $d^{-1}$). As consolidation proceeds, the cases with larger λ undergo a more concentrated decay near the inflection point and a faster mid-to-late decline in discharge capacity, so their reductions gradually catch up and overtake; by 500 d the reduction for λ = 0.02 $d^{-1}$ (about 1.71 points) exceeds that for λ = 0.005 $d^{-1}$ (about 1.39 points), and the curves cross in the mid-to-late stage. For the present parameter range all reductions remain within about two percentage points and reconverge as every case approaches full consolidation. Thus, with the inflection time fixed, λ mainly governs when the degradation-induced lag becomes concentrated; its effect is limited in magnitude but stage-dependent, and should not be neglected for long service periods or high target degrees of consolidation.

## 5.3 Effect of the Decay-Amplitude Parameter β

The decay-amplitude parameter β determines the ultimate proportion by which the drain permeability decays. Starting from the baseline β ≈ 0.51, five cases with β = 0.2, 0.35, 0.51, 0.65 and 0.8 were analysed, corresponding to residual discharge capacities of 80%, 65%, 49%, 35% and 20% of the initial value, respectively, with the decay rate λ and inflection time $t_0$ held constant; the resulting data are given in Table 9 and the trends in Figure 9.

*Table 9: Difference in the degree of consolidation relative to the constant-$k_w$ case for different decay-amplitude parameters β (percentage points).*

| t (d) | β=0.2 | β=0.35 | β=0.51 | β=0.65 | β=0.8 | Constant $k_w$ |
|---|---|---|---|---|---|---|
| 100 | −0.22 | −0.40 | −0.57 | −0.77 | −0.97 | 0 |
| 250 | −0.47 | −0.88 | −1.30 | −1.85 | −2.45 | 0 |
| 500 | −0.48 | −0.96 | −1.55 | −2.52 | −3.96 | 0 |

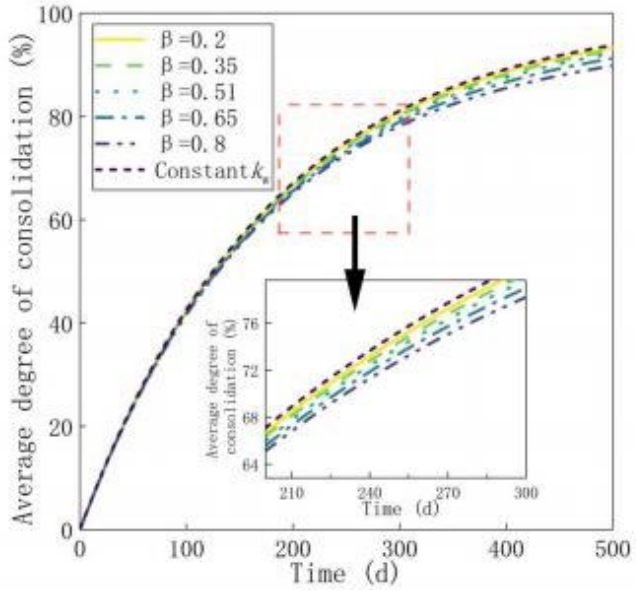


*Figure 9: Average degree of consolidation versus time for different decay-amplitude parameters β.*

Table 9 shows that increasing β markedly lowers the long-term drainage efficiency of the drain, with a particularly strong effect on the late consolidation stage. After the rapid mid-stage decay, cases with larger β show a more pronounced drop in discharge capacity, a larger increase in well resistance and a greater reduction in consolidation rate; in the late stage, the β = 0.8 case retains only 20% of the initial discharge capacity, so well resistance increases sharply and the consolidation rate falls substantially, whereas the β = 0.2 case still retains 80% of its capacity and its consolidation rate declines only slightly. In the design of biodegradable-PVD materials, the ultimate degree of degradation should therefore be controlled reasonably to ensure that sufficient residual discharge capacity is retained until primary consolidation is complete; an upper limit on β can be determined quantitatively from the engineering requirements on the degree of consolidation and post-construction settlement. It should be noted that, within the present parameter range, the differences in the degree of consolidation relative to the constant-$k_w$ case are of the order of a few percentage points and not numerically prominent. Their effects, however, differ in nature: the effect of β accumulates continuously with the consolidation period and is especially pronounced in the late stage, whereas the effect of λ mainly changes the timing at which the degradation-induced lag appears and is stage-dependent with a crossover (see Section 5.2). When the material degrades faster, the residual discharge capacity is lower, or the construction period is longer, the degradation effect increases significantly. Hence, although its magnitude is limited in this example, the degradation of biodegradable PVDs should not be neglected in material selection and construction-period matching, and in particular sufficient residual discharge capacity should be guaranteed until primary consolidation is complete.

### 5.4 Long-Term Settlement Prediction

On the basis of the validated parameter system, and keeping the domain size, boundary conditions, constitutive model, material parameters, loading mode and decay function unchanged, the calculation period was extended from 500 d to 1000 d for long-term settlement prediction, compared with the field settlement data in Figure 10. The simulated settlement at 200 d, 500 d and 1000 d is 540.0 mm, 743.4 mm and 787.8 mm, respectively, corresponding to an average degree of consolidation of about 98.7% at 1000 d. The settlement can be roughly divided into a rapid-settlement stage (0–200 d), a transitional stage (200–500 d) and a late stabilisation stage (500–1000 d): the late-stage increment is only about 44 mm and the curve gradually flattens. The results indicate that, although the drain discharge capacity decays with time, effective drainage is maintained during the primary-consolidation stage, so that the long-term settlement continues to develop and consolidation is essentially complete. It should be noted that the early field-measured settlement is clearly larger than the calculated value; it is therefore recommended that the soil compression modulus, coefficient of consolidation, permeability and loading history be back-analysed against measured data to improve the accuracy of the predicted early-stage settlement rate and long-term settlement.

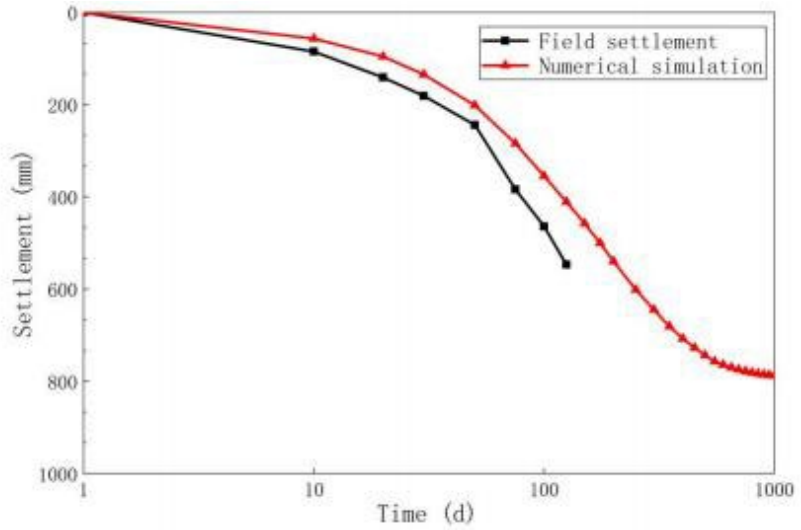


*Figure 10: Development of the long-term foundation settlement.*

# 6 Conclusions

An FE consolidation model accounting for the time-dependent decay of the drain equivalent permeability was established and applied, with the dredged silty-clay foundation at Meishan Port, Ningbo, as an example, to validation, parametric analysis and long-term prediction. The main conclusions are as follows.

(1) Based on laboratory accelerated-degradation and discharge-capacity test data, a logistic function with upper and lower asymptotes was used to formulate the time-dependent discharge-capacity decay equation; its fitting accuracy ($R^2 = 0.970$) is markedly better than that of the conventional exponential model, and it reasonably reflects the residual discharge capacity at the late stage. Through Darcy's law and the equivalent-hydraulic-radius method it was converted into a drain equivalent-permeability decay function $k_w(t) = k_w 0 f(t)$, quantitatively linking the material-degradation phenomenon to the consolidation-calculation parameters.

(2) To address the inability of general-purpose FE software to vary a parameter continuously with time, a staged-assignment method was proposed, approximating the continuous decay curve by a step function together with non-uniform time steps and a stage-doubling convergence check; the approximation error is of order $O(\Delta t)$ and controllable within an engineering-acceptable range. The method is generally applicable to any decay function and FE platform.

(3) The numerical model with a soft-soil non-linear constitutive law reproduces the overall trend of field settlement growth and pore-pressure dissipation reasonably well, but with some quantitative deviation (about 24.7% relative deviation in settlement at 120 d): the calculated settlement is generally lower than measured, and the predicted pore-pressure dissipation is slower. The model can be used to assess the consolidation-development trend and parameter sensitivity of dredged silty-clay foundations improved by biodegradable PVDs; for quantitative engineering prediction, the soil compression modulus, permeability and loading history should still be back-analysed against field monitoring data.

(4) The sensitivity analysis shows that reducing the drain spacing d markedly accelerates the overall consolidation rate. The decay-rate parameter $\lambda$ and the decay-amplitude parameter $\beta$ act in different ways: the effect of $\beta$ accumulates with the consolidation period and is especially pronounced in the late stage, whereas $\lambda$ mainly changes the timing at which the degradation-induced lag appears and is stage-dependent with a crossover. Both are limited in magnitude within the present parameter range (mostly within a few percentage points) but cannot be neglected for long service periods, high target degrees of consolidation or faster-degrading materials. The long-term prediction gives an average degree of consolidation of about 98.7% at 1000 d. In design, the material degradation rate, the effective service period and the foundation-treatment schedule should be considered together to keep the drain's discharge capacity sufficient during the primary-consolidation stage.

It should be noted that the present validation relies on a single field site and that the discharge-capacity decay law was fitted from a limited number of test points, so the long-term prediction beyond the monitoring window is indicative rather than definitive. Future work will extend the calibration to additional biodegradable-drain materials and soft-soil sites and couple the decay law with back-analysed soil parameters, so as to improve the quantitative predictive capability of the framework and support its wider use in green ground-improvement design.

Author Contributions: Conceptualization, L.C.; methodology, L.C.; software, L.C.; validation, L.C.; formal analysis, L.C.; investigation, L.C.; data curation, L.C.; writing—original draft preparation, L.C.; writing—review and editing, L.C.; supervision, L.C. All authors have read and agreed to the published version of the manuscript.

Funding: This research received no external funding.

Data Availability Statement: The data supporting the findings of this study — including the laboratory degradation and discharge-capacity test data, the converted drain-permeability values, the numerical simulation results, and the sensitivity-analysis data—are provided in the minimal dataset accompanying this article. Restrictions apply to the field settlement and excess-pore-pressure monitoring data at Meishan Port, which were obtained from the engineering project and are available from the corresponding author on reasonable request and with the permission of the project owner.

Conflicts of Interest: The authors declare no conflicts of interest.

Disclaimer/Publisher's Note: The statements, opinions and data contained in all publications are solely those of the individual author(s) and contributor(s), and the editor(s) disclaim responsibility for any injury to people or property resulting from any ideas, methods, instructions or products referred to in the content.

# References

[1] Nguyen T T, Indraratna B. Natural Fibre for Geotechnical Applications: Concepts, Achievements and Challenges[J]. Sustainability, 2023, 15(11): 8603.

[2] Berry P L, Wilkinson W B. The Radial Consolidation of Clay Soils[J]. Géotechnique, 1969, 19(2): 253-284.

[3] Hansbo S, Jamiolkowski M, Kok L. Consolidation by vertical drains[J]. Géotechnique, 1981, 31(1): 45-66.

[4] Onoue A. Consolidation by Vertical Drains Taking Well Resistance and Smear into Consideration[J]. Soils and Foundations, 1988, 28(4): 165-174.

[5] Kim R, Hong S J, Lee M J, et al. Time Dependent Well Resistance Factor of PVD[J]. Marine Georesources & Geotechnology, 2011, 29(2): 131-144.

[6] Indraratna B, Nguyen T T, Carter J, et al. Influence of biodegradable natural fibre drains on the radial consolidation of soft soil[J]. Computers and Geotechnics, 2016, 78: 171-180.

[7] Walker R, Indraratna B, Rujikiatkamjorn C. Vertical drain consolidation with non-Darcian flow and void-ratio-dependent compressibility and permeability[J]. Géotechnique, 2012, 62(11): 985-997.

[8] Chai J C, Shen S L, Miura N, et al. Simple Method of Modeling PVD-Improved Subsoil[J]. Journal of Geotechnical and Geoenvironmental Engineering, 2001, 127(11): 965-972.

[9] Walker R T R, Indraratna B. Application of spectral Galerkin method for multilayer consolidation of soft soils stabilised by vertical drains or stone columns[J]. Computers and Geotechnics, 2015, 69: 529-539.

[10] Nguyen T T, Indraratna B, Rujikiatkamjorn C. A numerical approach to modelling biodegradable vertical drains[J]. Environmental Geotechnics, 2022, 9(8): 515-523.

[11] Indraratna B, Redana I W. Numerical modeling of vertical drains with smear and well resistance installed in soft clay[J]. Canadian Geotechnical Journal, 2000, 37(1): 132-145.

[12] Yildiz A. Numerical modeling of vertical drains with advanced constitutive models[J]. Computers and Geotechnics, 2009, 36(6): 1072-1083.